AIAA SciTech Forum
6-10 January 2020, Orlando, FL
AIAA Scitech 2020 Forum

10.2514/6.2020-0838

Experimental and Numerical Investigation of a Roof-Scale Solar Chimney

Ladan Bahrainirad[*, 1], Md Kamrul Hasan[†, 2], Hermann F. Fasel[*, 3], Andreas Gross[†, 4]

[*]*Department of Aerospace and Mechanical Engineering, The University of Arizona, Tucson, AZ*
[†]*Department of Mechanical and Aerospace and Engineering, New Mexico State University, Las Cruces, NM*

This paper reports on an experimental investigation of the flow through the collector of a solar chimney power plant which has been constructed on the roof of the Aerospace and Mechanical Engineering building at the University of Arizona. This model contains a central chimney which is a long tubular structure located in the center, and a circular collector that employs the greenhouse effect to heat up the air under it. The chimney is 5.9m high and the collector radius measured from the center of the chimney is 4.13m. Measurements were carried out from April to June 2019. Several types of J thermocouples were mounted inside the collector at various radial locations to measure the air temperature both near the ground and the ceiling of the collector. A hot-wire probe (anemometer) was employed to measure the airflow velocity under the collector near the chimney inlet. A traverse system was designed and constructed, which allows the anemometer to be moved in the radial and circumferential direction under the collector. The height of the probe position above the collector ground can be adjusted by rotating the probe support along its longitudinal axis. A digital analog conversion system was used to convert the thermocouple and hot-wire readouts into binary data for processing via a LabVIEW interface. In parallel to the experiments, high-fidelity numerical simulations are being carried out for the conditions of the experiments. The simulations show longitudinal flow structures near the collector outflow that likely result from a buoyancy driven instability.

I. Introduction

In recent years, the rapid growth of the global population, the increase in living standards, and the accompanying enormous expansion of the global economy are putting ever more pressure on the natural resources and the environment. To address this issue, many nations are trying to expand their renewable energy production. The most ubiquitous forms of renewable energy are large hydroelectric plants, wind farms, and solar farms. Solar farms come in two forms, concentrating solar power (CSP) and photovoltaic (PV). The solar chimney power plant technology is a promising alternative to CSP and PV. Solar chimney power plants absorb direct and diffused solar radiation and convert part of the solar energy into electrical power. The solar updraft tower power plant, also called solar chimney, makes use of the greenhouse effect and the chimney effect. The solar irradiation heats the ground under a collector. The ground releases the heat into the air under the collector. The hot air rises in a central chimney. Turbines at the chimney entry extract energy from the airstream and convert it into mechanical energy. Alternators convert the mechanical power into electricity. The solar chimney power plant is attractive because the power production scales with the product of collector area and chimney height. Another benefit is that the technology is simple. During the last few years a 1:33 scale model of the Manzanares solar chimney power plant prototype in Spain (which was operated in the 80s after the first oil crisis) has been constructed on the roof of the Aerospace and Mechanical Engineering building at the University of Arizona. The collector radius of the model measured from the center of the chimney is 4.13m. The chimney height is 5.9m.

The ground is hotter than the collector cover and as a result a buoyancy-driven instability can occur. The flow can also be subject to a viscous instability. The main goal of this research project is to take careful measurements of the flow field inside the collector of the solar chimney model and to investigate the ensuing flow instabilities. Depending on the size of the collector and the strength of the instability, the ensuing disturbance growth may lead to laminar turbulent transition of the flow inside the collector. For a plane Poiseuille flow with thermal stratification, the so-called Rayleigh-Benard-Poiseuille (RBP) instability can arise.[1] The instability can lead to the amplification of both two-dimensional and three-dimensional waves depending on the Reynolds and Rayleigh number.[2]

[1] PhD Student in Mechanical Engineering, AIAA Member
[2] Graduate Research Assistant, AIAA Member
[3] Professor, AIAA Associate Fellow
[4] Associate Professor, Senior Member AIAA

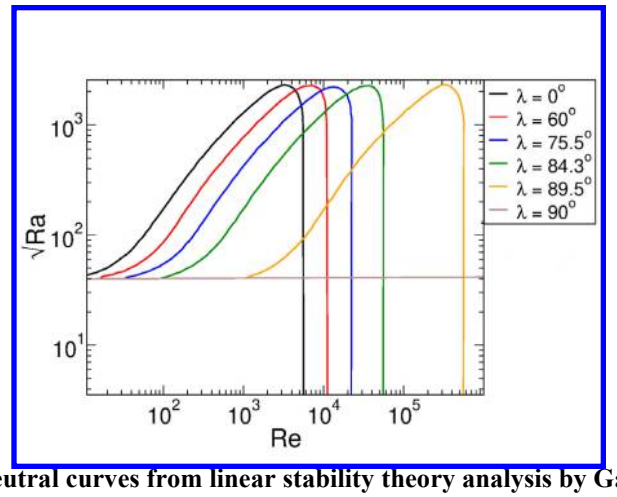

Figure 1. Neutral curves from linear stability theory analysis by Gage & Reid.[3]

The stability properties depend on four parameters: The Rayleigh number, $a = -\gamma g d^3 \Delta T/\kappa\nu$, the Reynolds number, $Re = Ud/2\nu$, the streamwise wave number, α, and the spanwise wavenumber β. The linear stability theory analysis by Gage & Reid[3] has shown that the neutral curve involves two different instability modes (see Fig. 1): At one end of the neutral curve ($Ra^* > 1708$ and Re^*<5400) the most amplified waves are completely three-dimensional (buoyancy-driven instability leading to longitudinal structures). At the other end of the neutral curve ($Ra^* < 1708$ and Re^*>5400), the most amplified waves are two-dimensional (viscosity-driven Tollmien-Schlichting instability leading to transverse structures). A linear stability theory analysis showed that the most critical disturbances for RBP flow are either two-dimensional transverse or longitudinal modes, and that there is no marginally stable flow for which truly three-dimensional disturbances are neutrally stable. Previous studies[4] showed that the lateral extent of the channel can raise the critical Rayleigh number for longitudinal rolls, such that transversal rolls are favored for small Reynolds numbers. A weakly nonlinear expansion up to cubic order has been considered by Nicolas et al.[5] It was found that the neutral curve was valid only for Re > 5000, and that there were three distinct critical transverse modes for Re less than 5000.[6] The longitudinal rolls are prevalent for $0 \leq Re < Re^*$, while a Tollmien-Schlichting instability becomes the prevalent mode for $Re > Re^*$. For certain parameter combinations, mixed instabilities (buoyancy-driven and Tollmien-Schlichting) can occur. Carriere & Monkewitz[7] took a closer look at the transition from convective to absolute instability in RBP flow and found that the mode reaching zero-group velocity always corresponds to transverse waves. However, the flow was found to remain convectively unstable with respect to pure longitudinal waves for all non-zero Reynolds numbers.

A solar chimney power plant model has been constructed on the roof of the Aerospace and Mechanical Engineering Department at the University of Arizona (UA). This model has two main components: (i) a central chimney, which is a long tubular structure which is located in the center and (ii) a circular greenhouse collector. The collector employs the greenhouse effect to heat up the air inside. The wall-normal temperature gradient between the ground and the collector ceiling results in a buoyancy force which can lead to a buoyancy-driven instability. The flow inside the collector accelerates in the radial direction toward the chimney. Thus, the Reynolds number rises and can potentially exceed the critical value for viscous instability to occur. Very low-amplitude environmental disturbances could grow by orders of magnitude as a result of the hydrodynamic instability mechanisms. Instability waves can reach large (non-linear) amplitudes and may develop further into vortical flow structures and finally result in laminar turbulent transition inside the collector. The main goal of this research project is to take careful scientific measurements of the flow field, temperature and velocity, in the collector of the solar chimney model and to study and investigate the ensuing flow instabilities. Furthermore, the measurements will provide guidance for numerical simulations that are being carried out in parallel with the experiments.

II. Experimental Set-Up and Instrumentation

The following section describes the experimental set-up and instrumentation for the temperature measurements. The radius of the collector and chimney is 4.1 m and 0.15 m, respectively, and the chimney height is 5.9 m (see Fig. 2). The collector cover is transparent and mounted above a cement plate with half inch thickness that is painted in black to collect the largest possible amount of solar energy and to maximize the heat transfer from the hot cement to the air inside the collector. A fiberglass pipe with inner diameter 0.3 m, was used as a chimney; the thermal conductivity of the fiberglass is very low, which helps minimize the heat loss from the chimney to the surroundings.

The aerodynamic forces acting on the chimney were calculated for a wind speed of up to 120mph. Two sets of stainless-steel guy wires were employed to hold the chimney upright. The system has double redundancy. Should either set fail, the chimney will not fall. In addition, the chimney is held at the base by a metal brace. To reduce the intensity of the van Karman vortex shedding during high winds, aluminum profiles were wrapped around the upper half of the chimney. At the bottom of the chimney, a cone made of fiberglass was installed to connect the chimney and collector and smoothly guide the flow into the chimney. Inside the cone is a symmetric spike-shaped body that also assistants in guiding the flow into the chimney. The cone has an access door which allows for the installation of a turbine and a generator if needed.

Figure 3 shows a schematic of the solar chimney collector sitting on the cement plate absorber. Most of the collector panels were made from a plastic greenhouse cover material. This material was found to be difficult to maintain. Therefore, recently one of the plastic panels was replaced by a glass panel. The collector panels are at a distance of 6.6 cm from the ground. All collector temperature and velocity measurements presented in this paper were taken under this glass panel. To measure the air temperature inside the collector, eight type J thermocouples were placed at different radial locations. Figure 4 (left) shows the thermocouples inside the collector before the glass panel was installed. For each location, one thermocouple was attached to the ground and another thermocouple was placed very close to the glass cover. To prevent circumferential flow into and out of the instrumented section, two dividers were added at the azimuthal fringes of the instrumented panel as shown in Fig. 4 (left).

Figure 2. Solar chimney power plant model on the roof of the Aerospace and Mechanical Engineering building at the University of Arizona.

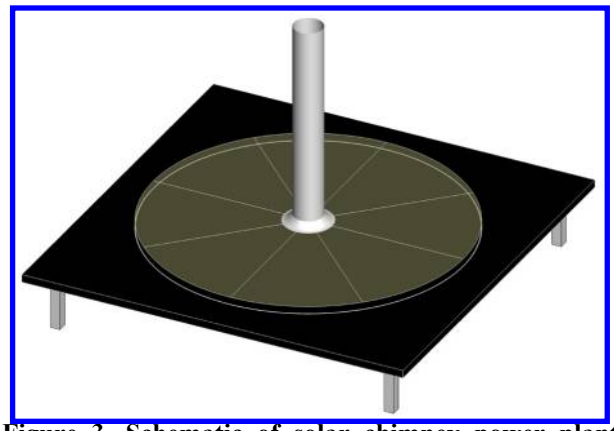

Figure 3. Schematic of solar chimney power plant model.

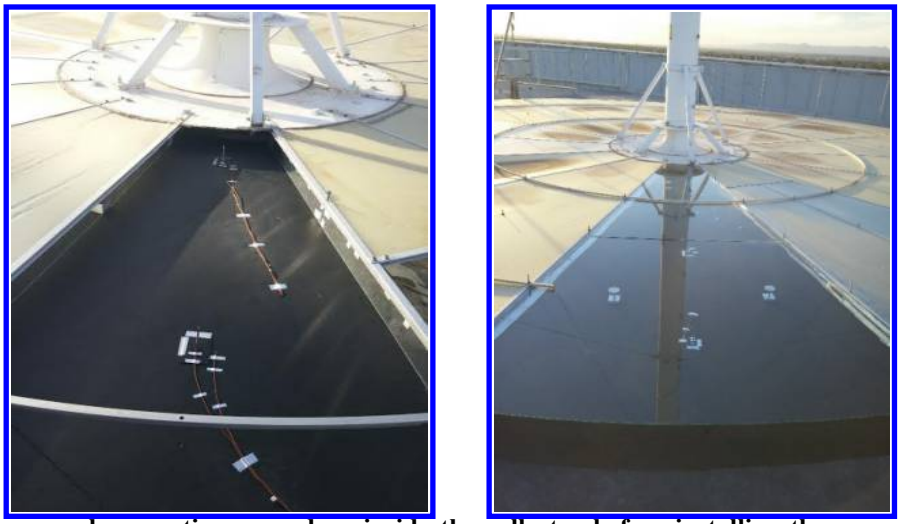

Figure 4. Thermocouple mounting procedure inside the collector before installing the cover (left) and with cover on (right). Two thermocouples were placed at each location (one on the ground and one on the top close to the collector cover).

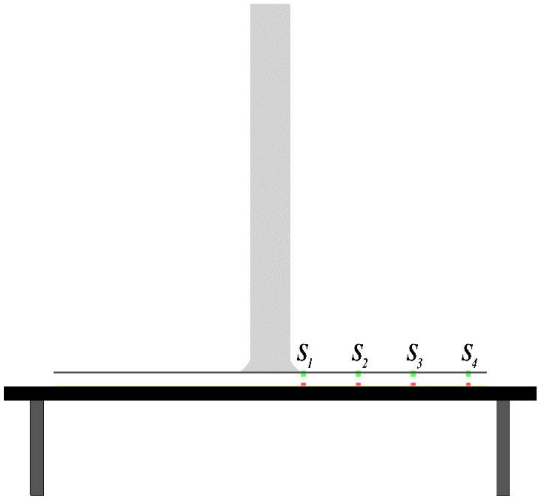

Figure 5. Schematic side-view of the solar chimney model with thermocouples in position 1, 2, 3, and 4.

Figure 4 (right) shows the position of the thermocouples inside the collector after the glass cover had been installed. Figure 5 illustrates the position of the thermocouples inside the collector. The thermocouples S1 are placed in location 1 on the ground and under the glass on the top, the thermocouples S2 are at location 2 and so on. As shown in Fig. 5, thermocouples S4 are placed close to the collector inlet at r = 3.167 m, thermocouples S3 are placed at r = 2.278 m, thermocouples S2 are placed at r= 2.0 m and thermocouples S1 are placed close to the chimney inlet at r = 0.5 m. The thermocouples located at the green points are used to measure the temperature at the bottom of the glass panel. The red ones are placed near the ground.

Figure 6 illustrates the experimental instrumentation used for the temperature measurements. Eight type J (Fe-Cu-Ni) thermocouples were employed to measure the air temperature inside the collector. Accordingly, four locations were chosen for the placement of the thermocouples in the radial direction. The diameter of the tip of the thermocouples is 0.25mm. A digital analog conversion (DAQ) system together with LabView were used to record the temperature data (see Fig. 6a). The analog signals from the thermocouples were converted with a National Instruments SCXI-1303 unit (Fig. 7b), which is designed to minimize errors caused by thermal gradients. A box with cooling fans was built to protect the instrumentation from the weather.

(a) (b)

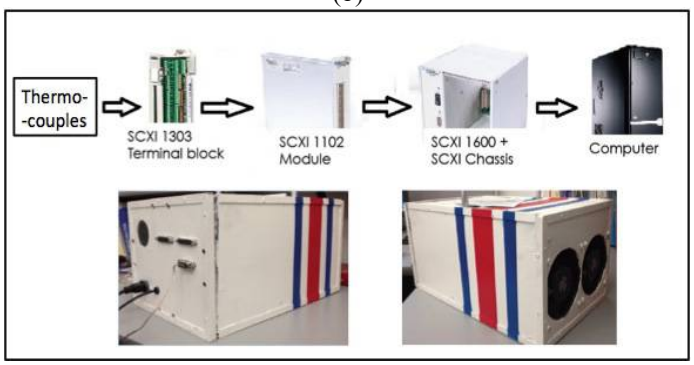

Figure 6. (a) Type J Thermocouple, (b) data acquisition device.

IV. Part I: Temperate Measurements Inside the Collector

The first section of the discussion is dedicated to the temperature measurements inside the collector at various radial locations. The experimental results were collected from April to June 2019 under different environmental conditions (sunny and rainy days). Figure 7 shows the results for April 26 which was a sunny day. On this day, data was collected from 11am on April 26th to 2:15am on April 27th. Figure 7(a) shows the measured temperatures for the ground and Fig. 7(b) illustrates the collected temperatures near the top cover. A comparison between the temperatures on the ground and on the top is shown in Figs. 7c – 7f.

The results confirm that the temperatures on the ground are much higher than the temperatures at the top (under the glass). Interestingly, sensor 2 shows the highest temperature, while the temperature reading for thermocouple 4 is the lowest among the four thermocouples on the ground.

May 9th was a rainy day and data were collected from 12:18pm to 8:17pm (see Fig. 8). Note that the thermocouples 1G, 1T are close to the inlet. Consequently, there was rain on the panel, and the panel was not able to warm up. Also, the solar radiation was much lower than on a sunny day. As can be seen, the difference between the panel and the ground temperature is decreased. For the same day, the ground temperature (solid line, see Figs. 8c, d, e, f) benefited from the previous sunny day. Stored heat energy from the previous day is released and heats up the air inside the collector.

Figure 9 illustrates the measured temperatures from 8:40am on June 13th to 10:40pm on June 14th. Figure 9(a) reveals that the temperature for thermocouple 2 is higher compared to the other thermocouples. A comparison between the temperatures at the top and the ground shows that the ground temperature is 15 °C higher than the temperature measured on the top. Figure 9(b) illustrates the temperatures recorded on the top. Thermocouples 2 and 3 are showing higher temperatures near the collector cover, and thermocouple 4 has the lowest temperature reading. It should be noted that the temperature remains constant for almost four hours after reaching its maximum for all positions.

Temporal mean of the temperature records at various radial locations (both on the top and the bottom) over a time interval from 12pm to 4pm on June 14th is presented in Fig. 10. Figure 10 reveals that the temperature is increasing as the air approaches the collector outflow (toward the inlet of the chimney). The temperature for the top cover, has the same trend except that there is a small jump for thermocouple 3. Overall, the temperature of air inside the collector increases by about 10 °C as the inlet of the chimney is approached. On a sunny day the temperature inside the collector increases from the ambient temperature of 38.4 °C at the outer periphery to a temperature of 80 °C halfway into the collector.

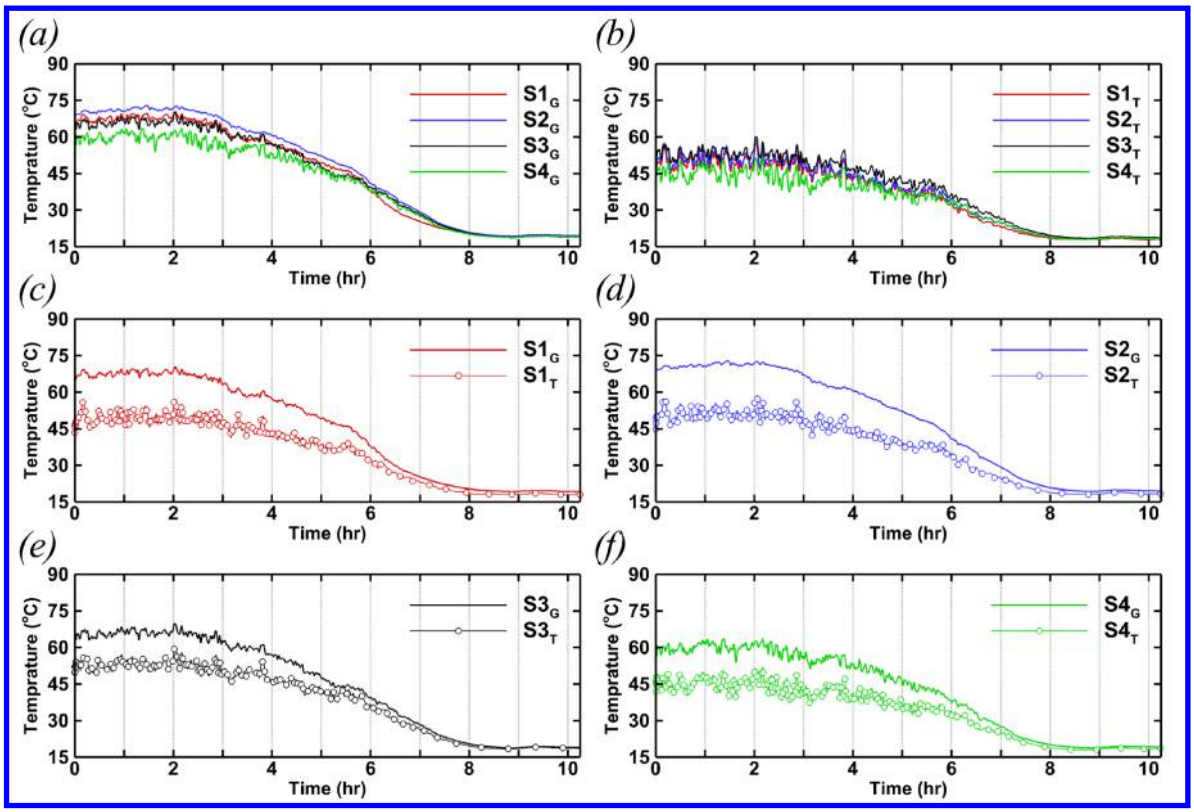

Figure 7. Measured temperatures on the ground (a) and near the glass panel (b). (c) Temperatures for S1 at $r = 0.5\ m$; (d) Temperatures for S2 at $r = 1.38\ m$; (e) Temperatures for S3 at $r = 2.27\ m$; (f) Temperatures for S4 at $r = 3.16$ m.

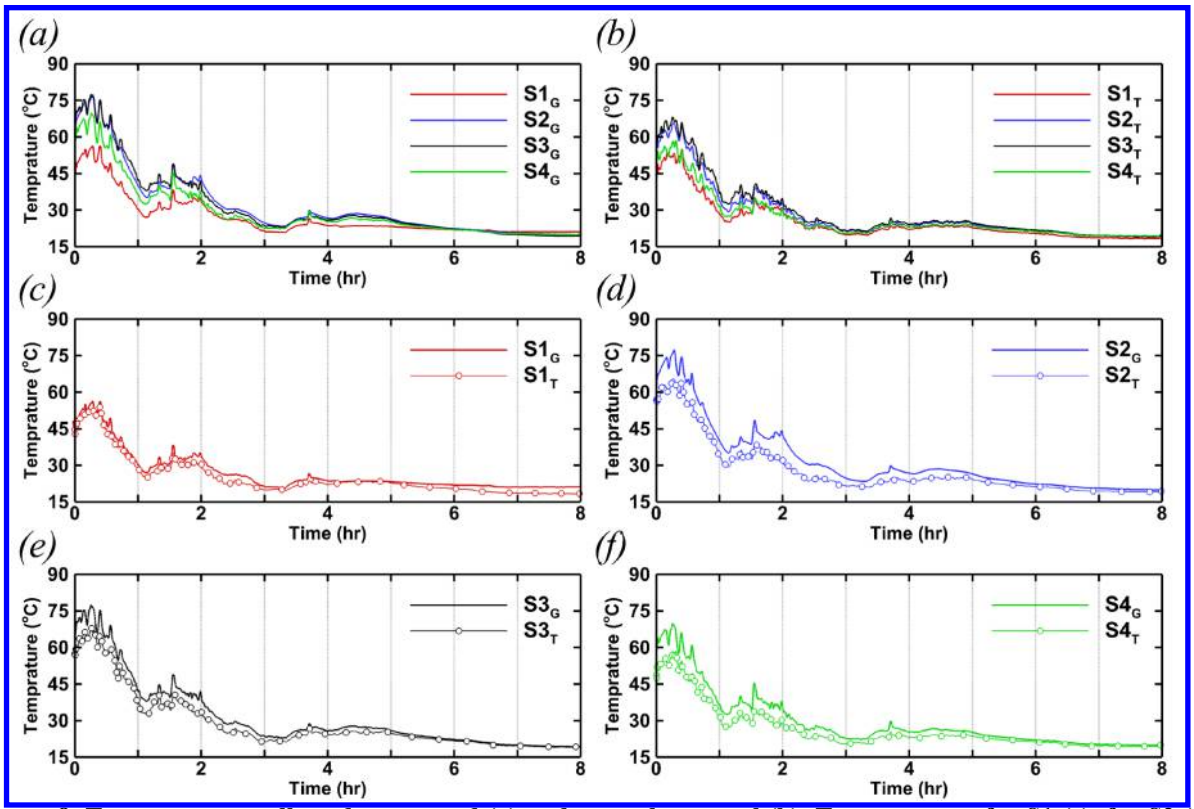

Figure 8. Temperatures collected on ground (a) and near glass panel (b). Temperatures for S1 (c), for S2 (d), for S3 (e), and for S4 (f).

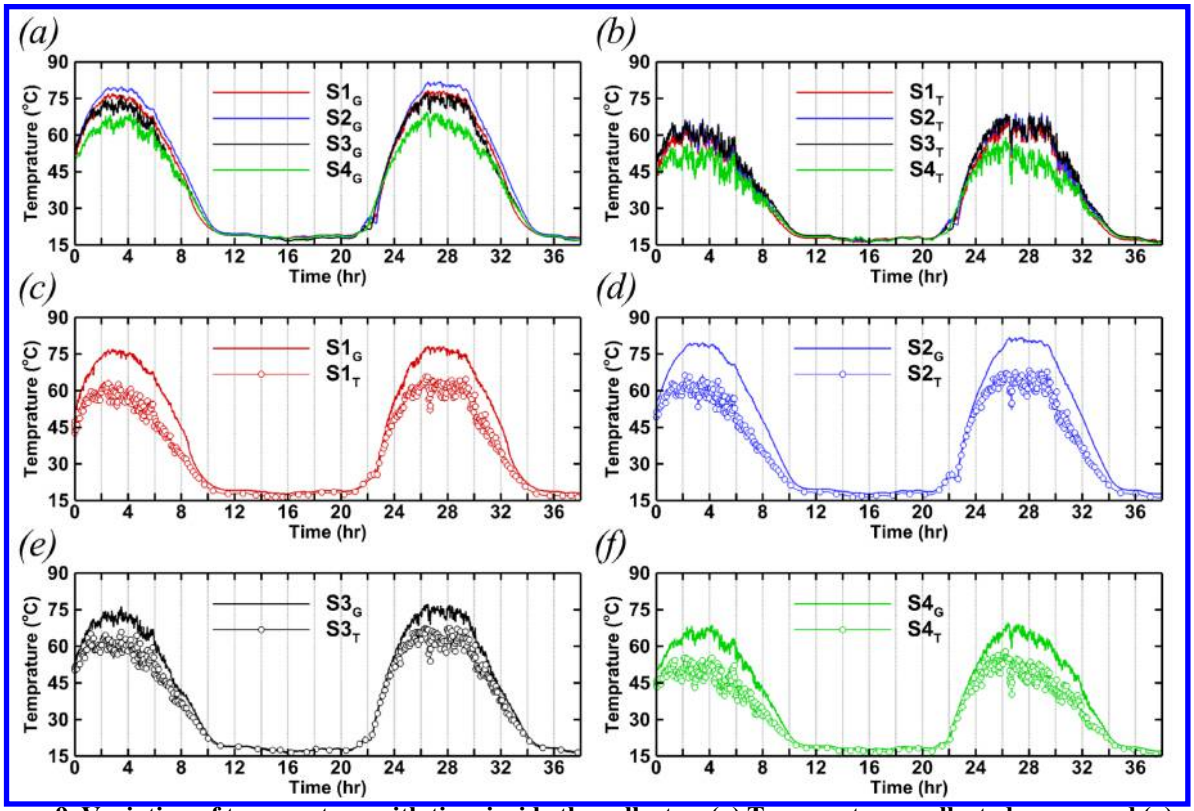

Figure 9. Variation of temperature with time inside the collector. (a) Temperatures collected on ground (a) and near glass panel (b). (c-f) Comparison of temperatures on ground and near collector cover.

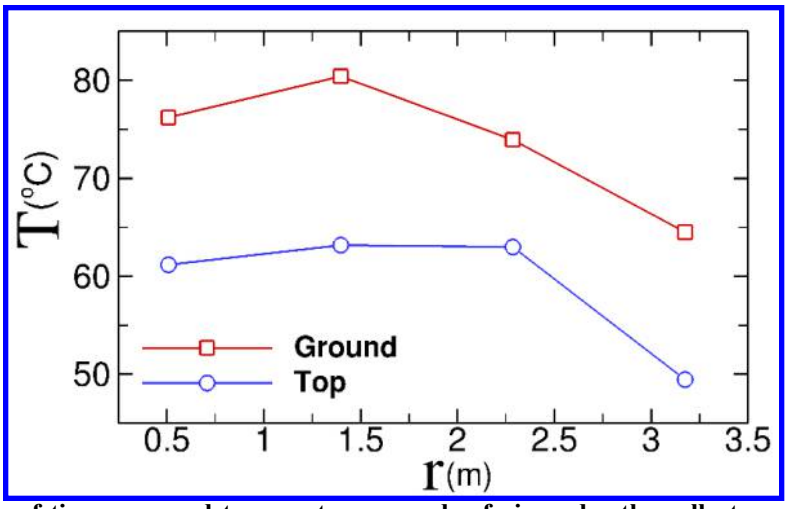

Figure 10. Variation of time-averaged temperature records of air under the collector with radial direction. Temperature measurements were averaged over a time period from 12pm to 4pm on June 14th.

The velocity of the air is inversely proportional to the collector radius. By considering the continuity for the air flowing through the collector towards the chimney, the velocity in the collector in different radius (r) can be approximated by

$$V = \frac{\pi R_{ch}^2 V_{ch}}{2\pi r h},$$

where h is the height of the collector, R_{ch} is the radius of the chimney, and V_{ch} is the velocity inside the chimney. The following equation is used to obtain an approximate value for the chimney updraft velocity, V_{ch}:

$$\Delta p = \rho_a g H_{ch} \frac{\Delta T}{T_a} = \frac{1}{2}\rho_a V_{ch}^2 .$$

Here, Δp is the difference between the pressure at the chimney base and the surroundings, T_a is the ambient temperature, and H_{ch} is the height of the chimney.

Figure 11 illustrates the variation of air velocity under the collector for June 14th. In Fig. 11, the velocity at different radial locations is plotted versus time for a time interval from 2pm to 3:10pm on June 14th. The velocity at $r = 0.5\ m$ (location 1) has the largest fluctuation compared to the other locations.

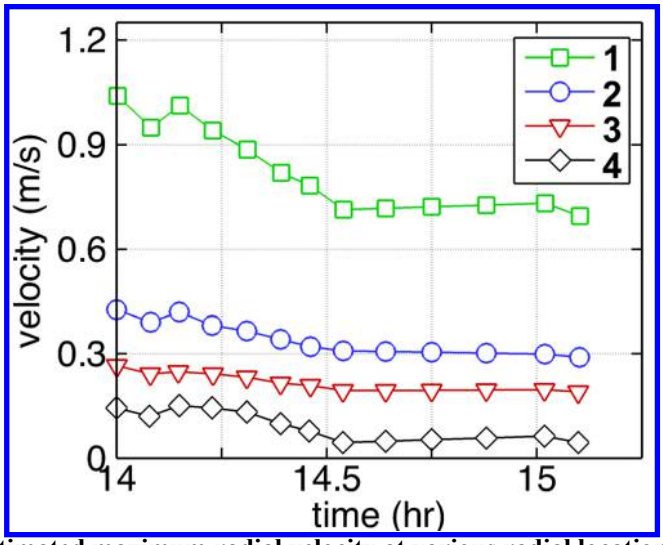

Figure 11. Estimated maximum radial velocity at various radial locations for June 14.

V. Part II: Hot-Wire Velocity Measurements

To measure the airflow velocity under the collector of the solar chimney model we decided to use a hot-wire anemometer. The hot-wire anemometer is made of a very thin Tungsten wire. The sensor is heated to some temperature above the ambient. Air flowing past the wire cools the wire. As the electrical resistance of most metals is dependent on the temperature of the wire, a relationship can be obtained between the resistance of the wire and the flow speed.

One of the main challenges was the necessity to accurately position the hot-wire probe under the collector. This was accomplished by designing and constructing a traverse system to move the probe around as shown in Fig. 12. The traverse system was designed to allow the probe to be moved from the inlet of the collector all the way to the inlet of the chimney. Additionally, the system allows the probe to be moved in the circumferential direction. The design was guided by considerations aimed at minimizing the disturbance of the flow by the mounting. Various components of the traverse system are shown in Fig. 12.

Figure 13 shows the traverse system placed inside the collector. The rails which allow for motion in the radial and circumferential direction can be seen. The vertical position of the probe was controlled by rotating the probe around the axis of the radial rail. In order to measure the velocity near the entrance of the chimney, in our latest version the length of the radial steel rail was extended to 12 ft and the probe holder was made adjustable (see Fig. 14).

Two modules for measuring the velocity and temperatures were integrated into a new Data Acquisition System (DAQ) from National Instruments. The DAQ system has a Compact DAQ Ethernet chassis which was placed inside a waterproof military storage box as shown in Fig. 15. A fan was mounted on one side of the box to cool the components. A LabVIEW interface was developed for visualizing and recording the synchronized velocity and temperature measurements. The hotwire probe was mounted on the traverse system and a series of measurements were carried out inside the collector.

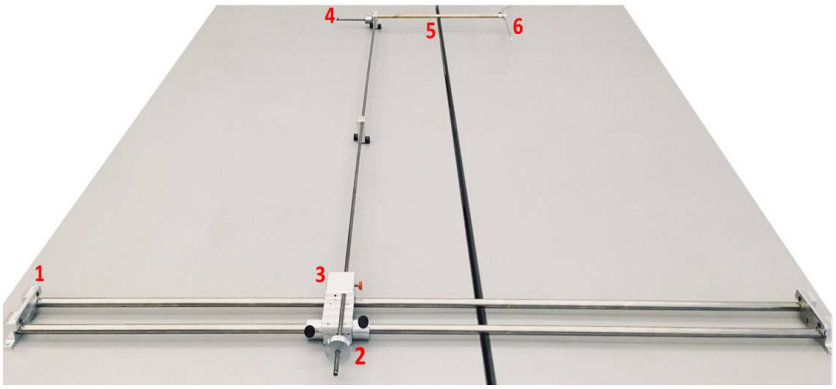

Figure 12. Illustration of traverse system. 1) Two Base-Mounted Shaft Supports used to move the rails in azimuthal direction 2) The Knob used for the rotation of the steel bar 3) Two bearings used to move the rails in azimuthal direction, and a holder used for holding steel bar in normal direction. 4) Counterweight used for balance 5) Sensor holder (length: 40cm) 6) Hot-wire sensor.

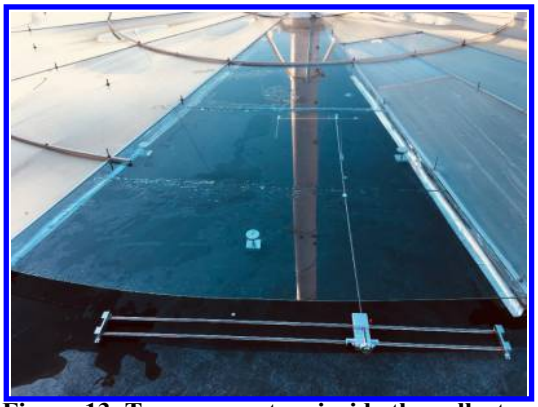

Figure 13. Traverse system inside the collector.

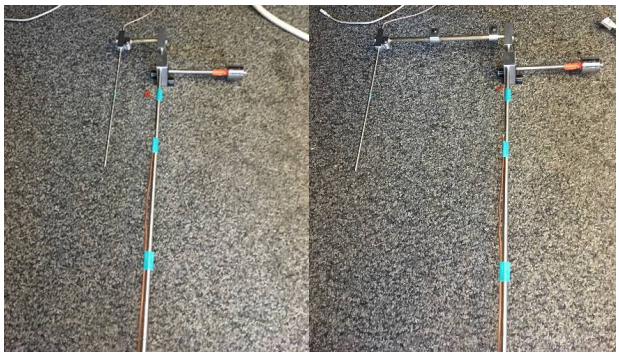

Figure 14. Adjustable hot-wire sensor holder.

Figure 15. Data Acquisition System consists of velocity and temperature modules as well as a chassis, placed inside a waterproof military storage box. A fan was added to cool the components.

The hot-wire probe requires calibration for providing reliable and repeatable measurements. The calibration of the hot-wire was accomplished using the Dantec Dynamics hot-wire calibrator, which is shown in Fig. 16. The calibrator produces a free jet, where the probe is placed during calibration. In the calibration process, output voltages (E) are obtained for known jet velocities (V). Subsequently, the resultant data pairs (E, V) are plotted to obtain the calibration curve for the hot-wire sensor. Figure 17 shows the calibration curve of the current hot-wire probe (data and fitted curve). The x-axis is the known target jet velocity and the y-axis represents the recorded hot-wire probe voltage. The minimum velocity is about $V = 0.1$ m/s and corresponds to a voltage of $E = 1.36$ V.

Preliminary hot-wire measurements inside the collector are presented in Fig. 18. The hot-wire probe was placed at the collector half-height at a distance of 24 cm from the entrance of the chimney. Data from the hot-wire probe and thermocouple sensor were recorded by LabVIEW at a 100 Hz sampling frequency over a period of 100 seconds. This procedure was repeated with about a 6-8 second gap in between. The hot-wire calibration was done at room temperature, which is different from the experiment. Therefore, the calibration curve in Fig. 17 was used with the aid of a correction coefficient in order to take into account the temperature difference between the calibration environment and the experiment.

Figure 18 shows the variation of the voltage recorded by the hot-wire (top plot), the velocity computed according to the calibration curve (middle plot), and the ambient temperature measured by a thermocouple sensor outside the collector (bottom plot) as a function of time. Since our thermocouple sensors were not long enough to be placed in close proximity of the hot-wire probe, we were not able to measure the temperature gradient. However, from our latest temperature measurements, we expect that it is about 15-20 C for this location.

Figure 16. Hot-wire calibration setup.

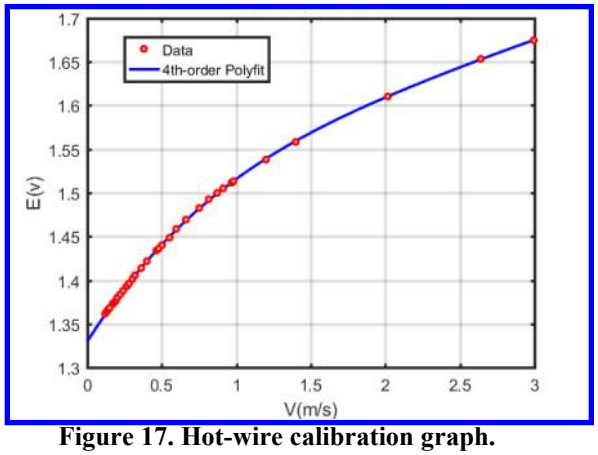

Figure 17. Hot-wire calibration graph.

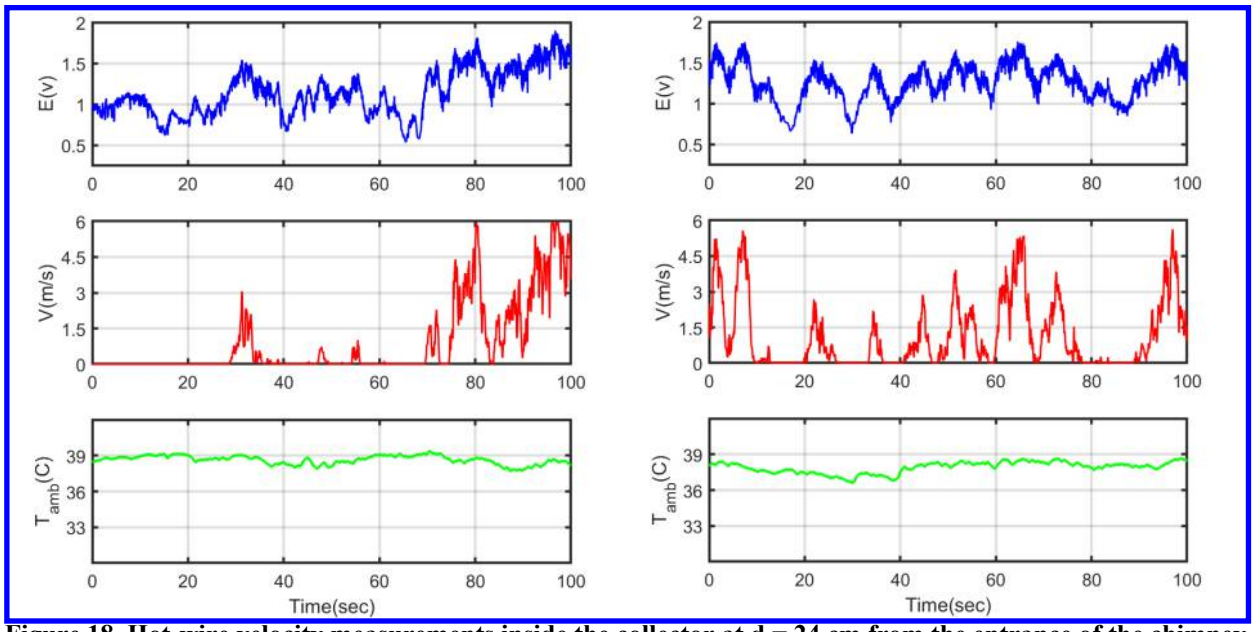

Figure 18. Hot-wire velocity measurements inside the collector at d = 24 cm from the entrance of the chimney. Shown are the variation of voltage recorded by the hot-wire (top), the velocity computed according to the calibration curve (middle) and the ambient temperature measured by a thermocouple sensor (bottom) as a function of time.

VI. Part III: Collector Simulation

First steps were taken to model the experiment using high-fidelity numerical simulations. An in-house developed computational fluid dynamics code[8] based on a finite volume method was employed to numerically investigate the flow physics inside the solar chimney model collector. An earlier simulation carried out by Fasel et al.[9] for the 1:30 scale model of the Manzanares plant was based on a reference Mach number of 0.001. This makes the numerical simulation very expensive since the time required for one flow-through was very high. Therefore, the reference Mach number was increased to 0.05. The collector half-height was chosen as reference length scale and the collector inflow velocity was taken as reference velocity scale. Based on this scaling the Reynolds number was Re = 721.1 and the Rayleigh number was $Ra = 23.87 \times 10^6$. According to Gage and Reid[3] when the Reynolds number is below $Re_c = 5{,}400$ and the Rayleigh number is above $Ra_c = 1{,}708$, buoyancy-driven instability occurs and 3-D waves with a wave angle of 90deg are most amplified.

Instantaneous iso-surfaces of Q=0.02 colored by the velocity magnitude exhibit eight longitudinal rolls as seen in Fig. 19a. An artificial disturbance was introduced near the collector inlet. The disturbances are growing in the streamwise direction (spatial growth) and develop into longitudinal structures. The structures appear to merge near the collector outlet.

(a) (b)

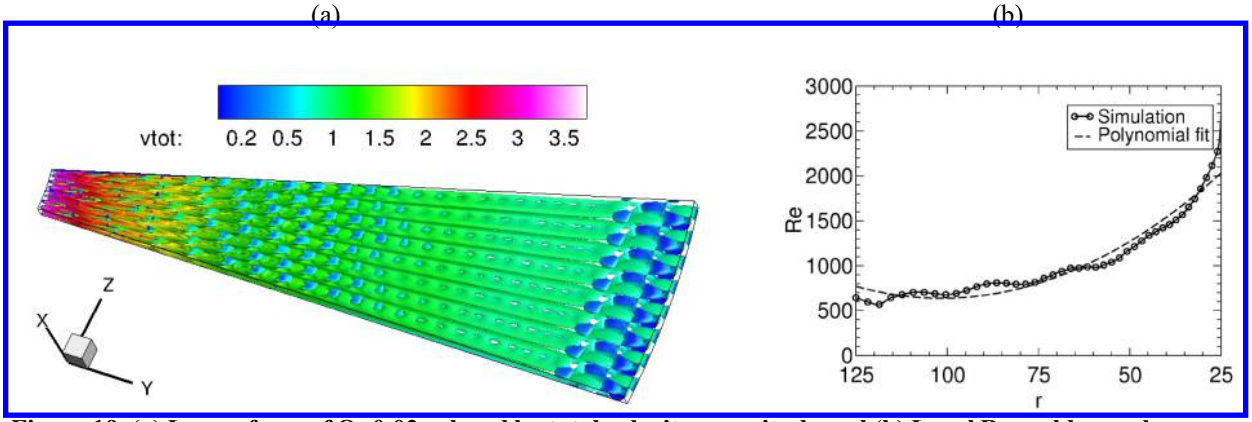

Figure 19. (a) Iso-surfaces of Q=0.02 colored by total velocity magnitude and (b) Local Reynolds number versus collector radius.

The flow accelerates very strongly in the streamwise direction because of continuity ($\rho v \propto 1/r$-relationship) and non-parallel effects become important. Since acceleration generally has a stabilizing effect[10] the inward radial RBP is expected to be more stable than the plane RBP flow especially near the collector outlet where the acceleration is very large. The local Reynolds number is plotted against the collector radius in Fig. 19b. The Reynolds number (or radial velocity) increases hyperbolically in the streamwise direction from $Re \approx 700$ (at the inlet) to about Re=2700 (at the outlet).

VII. Conclusion

The main objective of this work was to take scientific measurements of the temperature and velocity inside the collector of a solar chimney power plant model which was constructed at the University of Arizona and placed on the roof Aerospace and Mechanical Engineering building. Toward this end, the model was instrumented with temperature probes, namely type J thermocouples. Several thermocouples were installed inside the collector at various radial locations. Two thermocouples were used at each location, one was placed on the ground and the other one was placed near the collector top cover. The temperature measurements indicate a temperature differential as high as 15 K and a maximum temperature close to 80 °C. Further, it was shown that the temperature increases as the air approaches the inlet of the chimney. The second part of this research project was dedicated to measuring the air velocity inside the collector. This was accomplished by mounting a hot-wire probe on a traverse system which was designed and built at the University of Arizona. The hot-wire measurements were somewhat inconclusive. This was attributed to the open measurement environment. The ambient air (wind) velocity is of the same order or larger than the measured air velocity inside the collector. Therefore, in the future we will measure the local ambient wind velocity together with the solar irradiation. This will help us better interpret the hot-wire measurements. In addition, first steps were taken towards an accurate simulation of the flow through the collector for the conditions of the experiment. The simulation revealed streamwise structures which are an indication of buoyancy-driven instability.

Acknowledgments

This work was supported by the National Science Foundation (NSF) under grant number 1510717, with Dr. Ron Joslin serving as the program manager.

References

[1]Pretorius, J. P. Optimization and control of a large-scale solar chimney power plant. *PhD thesis*, University of Stellenbosch, 2007.

[2]Pastohr, H., Kornadt, O., and G¨urlebeck, K., "Numerical and analytical calculations of the temperature and flow field in the upwind power plant. International," *Journal of Energy Research*, Vol. 28, No. 6, pp. 495–510, 2004.

[3]Gage, K., and Reid, W., "The stability of thermally stratified plane poiseuille flow," *Journal of Fluid Mechanics*, Vol. 33, No. 1, pp. 21–32, 1968.

[4]Pearlstein, A. J., "On the two-dimensionality of the critical disturbances for stratified viscous plane parallel shear flows," *Physics of Fluids*, Vol. 28, pp. 751–753, 1985.

[5]Nicolas, X., Luijkx, J.-M., and Platten, J.-K., "Linear stability of mixed convection flows in horizontal rectangular channels of finite transversal extension heated from below," *International Journal of Heat and Mass Transfer*, Vol. 43, pp. 589–610, 2006.

[6]Fujimura, K., and Kelly, R., "Interaction between longitudinal convection rolls and transverse waves in unstably stratified plane poiseuille flow," *Physics of Fluids*, Vol. 7, pp. 68–79, 1995.

[7]Carriere, P., and Monkewitz, P. A., "Convective versus absolute instability in mixed rayleigh–benard–poiseuille convection," *Journal of Fluid Mechanics*, Vol. 384, pp. 243–262, 1999.

[8]Gross, A., and Fasel, H., "High-Order Accurate Numerical Method for Complex Flows," *AIAA Journal*, Vol. 46, No. 1, pp. 204-214, 2008.

[9]Fasel, H., Meng, F., Shams, E., and Gross, A., "CFD analysis for solar chimney power plants," *Solar Energy*, Vol. 98, pp. 12-22, 2013.

[10]Reed, H.L., and Saric, W.S., "Linear stability theory applied to boundary layers," *Annual Review of Fluid Mechanics*, Vol. 28, pp. 389-428, 1996.